

# Semantic Boundary Refinement by Joint Inference from Edges and Regions

Chao Yang\*  
University of Southern California  
chaoy@usc.edu

Guilin Liu\*  
George Mason University  
gliu2@gmu.edu

## Abstract

We study the problem of detecting boundaries for specific classes of objects. Our approach leverages recent advances in semantic segmentation and bottom-up boundary detection. We propose a mechanism for combining multiple sources of information: predicted segmentation masks, bottom-up contours, and a novel local class-specific boundary detector. These are jointly mapped to final category-specific boundary strength estimate by a trained classifier. In experiments on VOC2010 and Microsoft COCO data sets, our method dramatically outperforms recent prior work, for some classes doubling the accuracy of boundary prediction.

## 1. Introduction

Recognition of semantic categories in images has been one of the core tasks in computer vision since the beginning of the field. The details of tasks associated with recognition have evolved along with the complexity of available computation vision tools, from image classification (does the image contain instances of the category of interest) through bounding box detection, to category- and instance-level segmentation, where the goal is to label every pixel that belongs to categories of interest. In this latter task, one could reasonable devise different measures of accuracy. Recent work has largely focused on measures based on *region* accuracy, measured ultimately as a function of area of overlap. The accuracy of contours or boundaries, on the other hand, has received less attention.

The focus of our work presented in this paper is on *semantic boundary detection*: given an image, the goal is to predict where are boundaries that separate objects in a category of interest from everything else. This objective combines elements of semantic segmentation (since it is ultimately about category-aware partition of the image) and edge detection (since it deals with finding thin boundary elements rather than labeling regions). Both of these tasks have

seen significant advances in recent years, and one could consider directly combining predictions from state of the art semantic segmentation and state of the art non-semantic segmentation to yield semantic boundaries.

We show that such a combination could indeed produce a strong baseline, which for many classes far outperforms best reported results in the literature. However, we can do better, by refining the information that these two sources of information (regions and edges) give us about category-specific boundaries. The mechanism by which the information is fused is based on joint reasoning over semantic segmentation, bottom-up contours, and local semantic boundary classification; the parameters of this mechanism are learned from the data. A schematic overview of our approach, which we describe in detail in Section 3, is shown in Figure 1.

Other recent efforts on semantic contour detection, most notably [9] and [21], have also proposed ways to combine bottom-up (non-semantic) and top-down (semantic) information. Our approach differs both in the way these two sources of information are captured, and in the way they are combined. Experimental results on VOC 2012 and Microsoft COCO data sets show that the richer representation and the more sophisticated learning we propose pay off, yielding performance much higher than the previously established state of the art, both for category-specific and category-agnostic semantic boundary detection.

## 2. Background

Our work leverages recent results in two related recognition tasks: non-semantic contour detection and semantic segmentation.

**Non-specific boundary detection** There is a rich tradition of bottom-up, non-category specific edge or boundary detection in computer vision. For a long time, the problem lacked clear definition of what is the appropriate target for edge detection, or what is the appropriate evaluation measure; consequently there was no established data sets and associated benchmarks. Since the introduction of Berkeley Segmentation Dataset (BSDS) [17], modern work on

---

\*Equal Contribution.

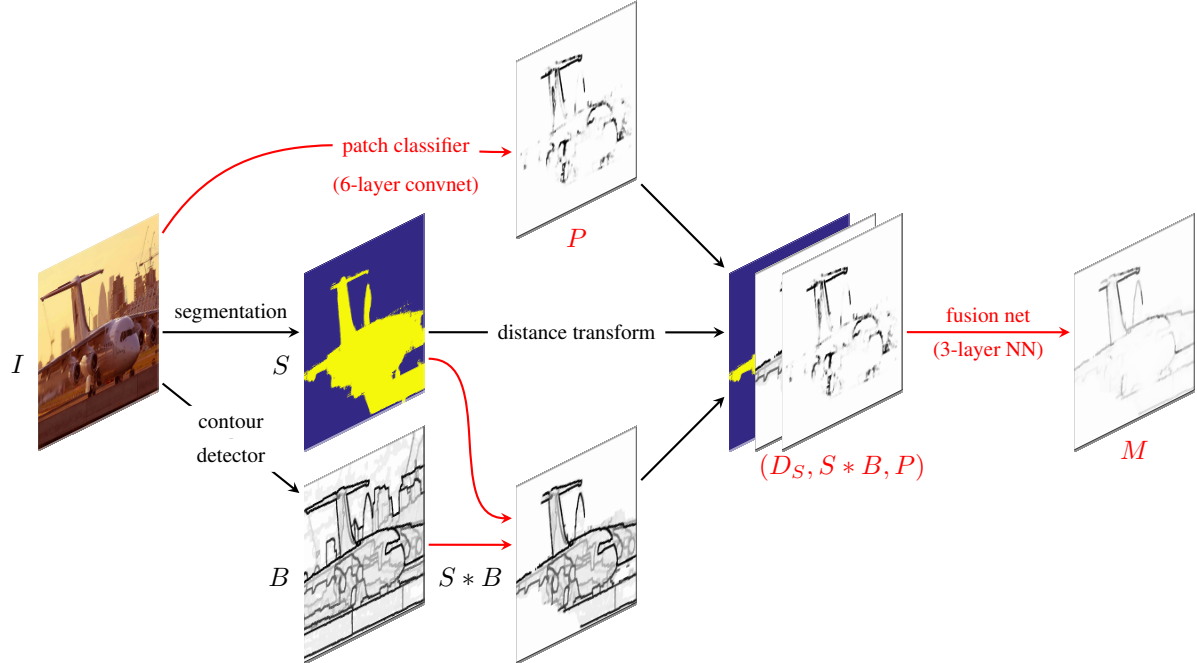


Figure 1. Overview of our semantic boundary detection pipeline.  $I$ : input image;  $S$ : class-specific figure/ground segmentation;  $B$ : non-semantic boundary map;  $S * B$ : masked boundary baseline;  $D_S$ : distance transform computed on edges of  $S$ ;  $P$ : class-specific boundary map computed by a patch classifier (6-layer fully convolutional convnet). The final class-specific boundary map  $M$  is obtained by applying a fusion classifier (2-layer neural network) on every pixel of a 3-channel map consisting of  $D_S$ ,  $S * B$  and  $P$ .

edge/boundary/contour detection largely relies on it as the source for well-defined boundary detection targets (multiple human boundary annotations) and as a vehicle for standardized evaluation. A typical output of a boundary detector consists of a probabilistic boundary map, in which a value in the range of [0,1] is interpreted as posterior probability of the pixel being on a boundary. Alternatively, this value can be interpreted as the perceptual strength of a boundary at the pixel. Some recently proposed methods [6, 19] achieve results that approach human level performance, with the standard evaluation protocol measuring precision-recall behavior (like F-measure and average precision). We chose to work with MCG [2, 19] the authors of which made pre-computed boundary maps available for all the data sets we worked with. This approach achieves F-measure of 0.74 on the BSDS test set, compared to F=0.81 for inter-human agreement. However, this is a *non-specific* boundary detector; it is not aware of object categories, and lumps all predicted boundaries together. Consequently, its performance as a category-specific, semantic boundary detector is abysmal; in [9] it is reported to achieve only 4% mean average precision on VOC data.

**Semantic segmentation** For many years semantic segmentation was dominated by variations on conditional random fields (CRFs), with increasingly complex high-order potentials [14, 8] and complex pre-processing and multi-

stage procedures [3, 22]. Subsequent progress in the field has been associated with approaches, using deep convolutional neural network (convnets) in conjunction with region proposals [10]. Even more recently, state of the art has been driven by feed-forward architectures that use the entire hierarchy of features computed in convnets to classify image elements [16, 18, 11, 12], with further improvement sometimes obtained by re-introducing CRFs on top of the convnet-based predictions [23, 4]. In experiments reported in this paper we have worked with the multiscale version of DeepLab-CRF architecture [5]. For each location in the image, it estimates category scores from features combined from multiple layers of a deep convnet. These are treated as unary potentials, and combined with RBF pairwise terms for all pairs of locations; MAP inference in the resulting dense CRF produces the final semantic labeling for the image.

The standard evaluation measure for semantic segmentation is intersection over union overlap between predicted vs. true pixels in each category, including background, averaged over categories (mean IoU). Trained on train+val portions of the VOC2012 data set [7], DeepLab-CRF achieves mean IoU of 71.6 on the test. We have experimented with training and testing this system on MS-COCO data set [15], which contains 60 additional categories and about an order of magnitude more images than VOC. With a DeepLab-CRF model trained on COCO-train and val-

uated on COCO-val, the mean IoU we could get was approximately 30%, significantly below that on VOC. We believe this faithfully reflects the performance level of leading approaches on COCO, with the gap relative to VOC probably due to increased complexity and confusability of some of the additional classes.

**Semantic boundary detection** There has been relatively little work directed at semantic boundary detection per se. The two most notable efforts are the Inverse Detectors method [9] and the more recent Situational Object Boundary Detection method [21]. In [9], bottom-up, non-specific boundary predictions are combined with coarse object detections in the form of bounding boxes. Our approach is similar in its use of bottom-up (non-semantic) and top-down (semantic) information, but we use semantic segmentation, rather than bounding box detectors, for the latter. Another difference is that we learn an expressive fusion classifier (neural network) that combines strength of bottom-up contours, distance to segmentation mask and a novel local semantic boundary detector, whereas in [9] the bottom-up contours are simply modulated by the weights predicted from class-specific detectors.

In [21] image-level features are used in a kind of gating mechanism that associates the image with a “situation”, which could be a class, sub-class, or class-agnostic scene type. Bottom-up, non-semantic edge detectors are trained separately on images clustered per situation; thus the only source of class-specificity is that clustering. In contrast to this work, we explicitly combine semantic and non-semantic information about contours, and learn a class-specific detector for each class. In Section 4 we show that our method outperforms both [21] and [9] by a wide margin.

### 3. Boundary refinement from regions and contours

We build the boundary detector for each class separately. Ultimately, our predictions are computed from three sources of information: semantic segmentation, non-specific (bottom-up) boundary detection, and class-specific local boundary detector. The first two components are based on existing tools developed by others, and the third one is learned. We describe the details for each of these components below.

#### 3.1. Segmentation baseline

A semantic segmentation system produces hypothesized masks for the category, and we could treat the contours of these masks as semantic boundary prediction. Note that these are hard 0/1 values, so in evaluation we obtain a single precision/recall point, that can be converted to average pre-

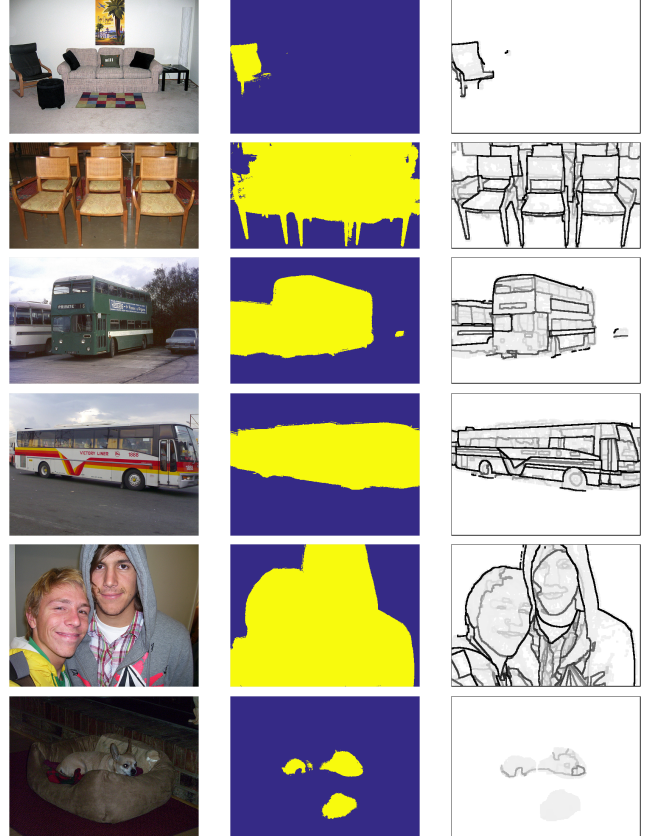


Figure 2. Segmentation and boundary baselines. Left: image  $I$ , middle: segmentation mask from DeepLab-CRF  $B$ , right: masked boundary  $B * S$  with  $B$  dilated by 5 pixels. From top to bottom: chair  $\times 2$ , bus  $\times 2$ , person, dog.

cision somewhat generously by extrapolating a piece-wise linear graph connecting this point to zero recall, full precision point.

#### 3.2. Masked boundary baseline

Non-category-specific, bottom-up boundary detectors produce strong responses for boundaries of many classes (and some interior boundaries), and because of their very low precision for any specific class they can not be used for category-specific detection. This was confirmed empirically in [9] for the detector in [1], and again in [21] for the detector in [6]; we observe this to be the case for our detector of choice [19] as well. However, we can attempt to boost the precision by masking the boundary map with class-specific segmentation mask, possibly dilated and/or with interior portion removed, to allow some “slack” in boundary localization. As we report in Section 4, which indeed produces a much improved semantic boundary detector.

Figure 2 illustrates these baselines for a few images. Typically, as can be seen here, the segmentation contour is good at suppressing interior boundaries, but could be

rather noisy in localizing exterior boundaries, and of course makes some mistakes in segmenting regions from wrong categories. Bottom-up contours masked with the segmentation can help suppress some of the spurious boundaries introduced by noisy segmentation mask, e.g., the pillow region labeled as dog, or portions of the background in the second chair example, in Figure 2. On the other hand, it also introduces spurious interior boundaries (e.g., examples of bus and person images in the figure). As we will see in experimental evaluation, trading off these sources of error leads to a similar level of performance by these two baselines. We'd like to change the tradeoff by taking the best that each of these baselines has to offer.

### 3.3. Local class-specific boundary detector

Although as we show in Section 4 the masked boundary baseline achieves results that on some classes outperform previous state of the art, it leaves much to be desired. Instead, we can train a class-specific boundary predictor from scratch. We implement it as a multi-layer convnet, trained to classify image patches as boundary or non-boundary for the class at hand.

The input to the patch classifier consists of a  $35 \times 35$  region with three color channels. Details of the network architecture are summarized in Table 1. Training examples are sampled from regions retained by the  $S * B$  masked boundary. The network is trained separately for each class.

	layer type	RF size	#units	stride
1	conv	4	96	1
2	max-pool	2		2
3	conv	3	256	1
4	max-pool	2		2
5	conv	4	64	1
7	ip		256	
8	ip		256	
9	ip		2	

Table 1. Architecture of the local boundary detector; “ip” stands for “inner product” (fully connected layers). The last ip layer is the classifier.

### 3.4. Information fusion

The three components described above each capture a different aspect of visual information. The segmentation mask is based on information collected over large portion of the image, but may offer poor localization of the boundaries. We can soften it, for instance by computing distance transform from the segmentation edges. Masked boundary map localizes the boundaries, but may suffer from low precision. The local boundary detector is trained on the right signal, but is based on limited view of the image due to its local nature.

Instead of choosing one of these components, we can learn a fusion mechanism that will combine their prediction.

The simplest form of such a mechanism would be a linear classifier, which simply assigns a weight to each channel. We found that better (modestly, but consistently) results are obtained by a non-linear classifier. Let  $\mathbf{x} = (d, b, c)$  be the triplet representing the input to the classifier at a pixel;  $d$  is the distance to nearest point on the boundary of segmentation mask for the category of interest (or a large default value if no such segmentation is present);  $b$  is the value of non-class-specific boundary map; and  $c$  is the boundary probability estimated by the local boundary detector. Then, our classifier predicts

$$\log \Pr(m = 1 | \mathbf{x}) \propto \mathbf{w}_3^T \sigma(\mathbf{w}_2^T \sigma(\mathbf{w}_1^T \mathbf{x} + \mathbf{b}_1) + \mathbf{b}_2) + b_3,$$

that is, it is a three-layer feedforward network with fully connected layers and sigmoid activation functions. We use 64 units in the first hidden layer (i.e.,  $\mathbf{w}_1 \in \mathbb{R}^{64}$ ) and 16 units in the second layer. We can also express it as a convnet, with filters of size  $1 \times 1$  throughout, and carry out the feedforward computation efficiently using standard tools for fully convolutional networks.

The entire pipeline for our semantic boundary detector is illustrated in Figure 1.

## 4. Experiments

We evaluate our fusion method, as well as its individual components, on two benchmark data sets: VOC 2012 and Microsoft COCO. In each of these, ground truth contains segmentation masks for object categories (20 for VOC, 80 for COCO). We used Caffe [13] to implement and apply the local patch classifier and the fusion network; DeepLab-CRF was also implemented in Caffe by the authors of [4].

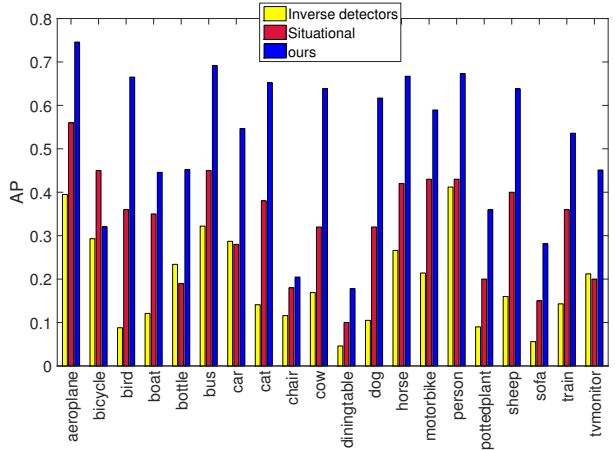


Figure 5. Per-class results on VOC2012, comparing the average precision of our fusion method to that of [9] and [21].

### 4.1. Results on VOC 2012

Following the SBD (semantic boundary detection) evaluation protocol in [9, 21] we used the 8,498 images as SBD



Figure 3. Examples of results with our pipeline on images in SBD test set. From left: input image, category-specific segmentation mask  $B$ , masked boundary  $B * S$ , patch classifier output  $P$ , and our final result with the fusion network. Target categories, from top: chair, bus  $\times 2$ , person  $\times 2$ , dog.

training set, and 2,820 as SBD test set. The remaining 676 images in VOC2012 were used as a validation/tuning set on which we evaluated models and tuned parameters.

The bottom-up MCG boundary detector was trained on BSDS, and used by us without modification. For the semantic segmentation model we trained DeepLab-CRF on the SBD training set (it was initialized with the 16-layer network pretrained on ImageNet classification task, obtained from [20]). After evaluating different parameter settings on the tuning set, we set the dilation radius for the segmentation mask to 5 pixels, and suppressed bottom-up contours with values below 0.05. We experimented with removing an interior portion of segmentation masks (by subtracting an eroded mask from the dilated mask) but found that it slightly hurt performance, due to the tendency of the segmentation algorithm to over-extend the masks, so that the removal of

the interior sometimes erases correct object boundaries; furthermore, since our evaluation protocol (see below) ignores interior contours, we do not gain much by removing them in this way.

Method	mean average precision
Inverse detectors [9]	19.9
Situational detectors [21]	31.6
Segmentation only $S$	45.8
Masked boundary $S * B$	46.0
Local patch classifier $P$	26.9
Fusion ( $D_s, S * B, P$ )	51.8

Table 2. Mean average precision for VOC2012 data set.

We evaluated average precision of different semantic boundary detectors per class, using the methodology and code from [9]. To make results comparable, we enabled

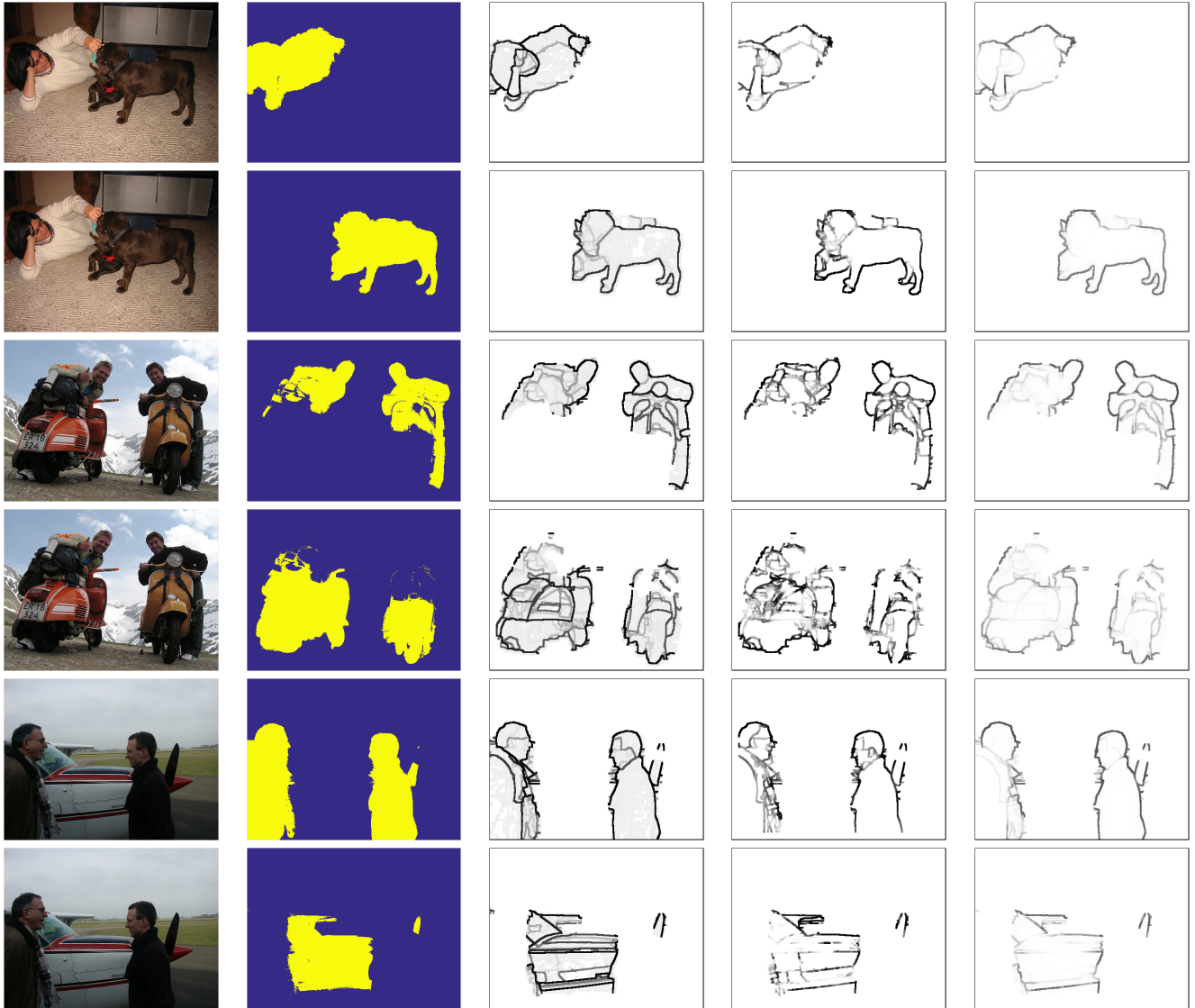


Figure 4. Additional examples, showing how multiple categories per image are handled. See caption of Figure 3 for details. Categories: person/dog, person/motorbike, person/aeroplane.

the default behavior which ignores interior contours (inside the ground truth masks for each class); this is somewhat unfavorable to our method which, as the examples in Figures 3, 4 demonstrate, is particularly good at suppressing interior contours.

The main result we report is the average precision (AP). The AP values averaged over 20 object categories are reported in Table 2. Figure 5 shows results per class. In all classes except bicycle and chair, our results are significantly better, sometimes almost doubling the AP. We hypothesize that bicycle and chair categories include many cases of thin structures, hard to capture by semantic segmentation and consequently by our fusion technique, that can only be partially salvaged if the underlying segmentation mask is bad.

## 4.2. Results on Microsoft COCO

Following the setup in [21] for COCO, we used the first 5,000 images from the `val` set as the test set for our experiments. We used the same bottom-up MCG contour model as in the VOC experiments; the 80-category DeepLab-CRF segmentation model trained on COCO `train` was obtained from the authors of [4]. In Table 3 we report the results of evaluating components of our system in this setup. The relative standing reflects that in Table 2, but all the numbers are lower, reflecting the increased difficulty of COCO compared to VOC.

Figure 6 shows the per-class AP with the fusion model, and the improvement obtained by the fusion model with re-

spect to the masked boundary baseline and the segmentation baseline, respectively, per class. While on all 80 classes the fusion outperforms the masked baseline, it loses to the segmentation baseline on a few classes; the worst four are backpack, tie, keyboard and refrigerator. These are also among the categories with the lowest boundary detection accuracy.

Method	mean average precision
Segmentation only $S$	36.9
Masked boundary $S * B$	38.5
Local patch classifier $P$	22.4
Fusion ( $D_s, S * B, P$ )	45.0

Table 3. Mean average precision for Microsoft COCO data set.

Neither [9] nor [21] include per-class AP results on COCO. However, [21] includes results of experiments (both on COCO and on VOC2012) in which ground truth boundaries for all categories are pooled, effectively defining a class-agnostic, foreground (any class) vs. background boundary detection tasks. These are evaluated against “class-agnostic” situational detectors, that are trained to predict such boundaries. We can emulate this experiment by max-pooling the predictions of our category-specific detectors for each pixel, forming a class-agnostic boundary detection map. A comparison of AP figures with our method and that of [21] is shown in Table 4, and the ROC curves are in Figure 7. It is clear that on this task, too, our fusion method performs significantly better than the prior work.

Method	VOC2012	COCO
Situational detectors [21]	42.6	43.4
Fusion ( $D_s, S * B, P$ )	61.2	58.9

Table 4. Average precision on class-agnostic object boundary detection task (all object boundaries, and predictors for all categories, pooled together).

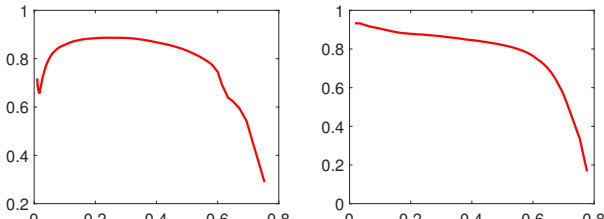


Figure 7. Precision-recall curves for the class-agnostic detection on COCO (left) and VOC (right).

## 5. Conclusions

We have proposed an architecture that fuses region- and edge-based information for category-specific semantic boundary detection. Our experiments demonstrate that such joint reasoning about regions and boundaries can improve boundary prediction results. Part of our pipeline relies

on previously proposed methods for semantic segmentation and for (non-specific) boundary detection; we also introduce two novel components: a multilayer convolutional network trained to predict boundary occurrence from local image evidence, and a two-layer network to combine multiple channels of information. The resulting fusion system works better than any of its parts alone, yielding performance significantly better than previously reported state of the art on VOC2012 and Microsoft COCO data sets.

Perhaps the most intriguing question that arises from our findings is whether better category-specific boundary predictions can help improve region prediction (semantic segmentation). We plan to explore this, as well as possible improvements through modifications in architecture.

## References

- [1] P. Arbelaez, M. Maire, C. Fowlkes, and J. Malik. Contour detection and hierarchical image segmentation. *IEEE TPAMI*, 33(5), 2011. 3
- [2] P. Arbelaez, J. Pont-Tuset, J. Barron, F. Marques, and J. Malik. Multiscale combinatorial grouping. In *CVPR*, 2014. 2
- [3] J. Carreira, R. Caseiro, J. Batista, and C. Sminchisescu. Semantic segmentation with second-order pooling. In *ECCV*. 2012. 2
- [4] L.-C. Chen, G. Papandreou, I. Kokkinos, K. Murphy, and A. L. Yuille. Semantic image segmentation with deep convolutional nets and fully connected crfs. In *ICLR*, 2014. 2, 4, 6
- [5] L.-C. Chen, G. Papandreou, I. Kokkinos, K. Murphy, and A. L. Yuille. Deeplab: Semantic image segmentation with deep convolutional nets, atrous convolution, and fully connected crfs. *arXiv preprint arXiv:1606.00915*, 2016. 2
- [6] P. Dollár and C. L. Zitnick. Structured forests for fast edge detection. In *ICCV*, 2013. 2, 3
- [7] M. Everingham, L. Van Gool, C. K. Williams, J. Winn, and A. Zisserman. The pascal visual object classes (voc) challenge. *IJCV*, 88(2), 2010. 2
- [8] J. M. Gonfaus, X. Boix, J. Van de Weijer, A. D. Bagdanov, J. Serrat, and J. Gonzalez. Harmony potentials for joint classification and segmentation. In *CVPR*, 2010. 2
- [9] B. Hariharan, P. Arbelaez, L. Bourdev, S. Maji, and J. Malik. Semantic contours from inverse detectors. In *ICCV*, 2011. 1, 2, 3, 4, 5, 7
- [10] B. Hariharan, P. Arbelaez, R. Girshick, and J. Malik. Simultaneous detection and segmentation. In *ECCV 2014*, 2014. 2
- [11] B. Hariharan, P. Arbelaez, R. Girshick, and J. Malik. Hypercolumns for object segmentation and fine-grained localization. In *CVPR*, 2015. 2
- [12] K. He, X. Zhang, S. Ren, and J. Sun. Deep residual learning for image recognition. In *Proceedings of the IEEE Conference on Computer Vision and Pattern Recognition*, pages 770–778, 2016. 2
- [13] Y. Jia, E. Shelhamer, J. Donahue, S. Karayev, J. Long, R. Girshick, S. Guadarrama, and T. Darrell. Caffe: Convolutional

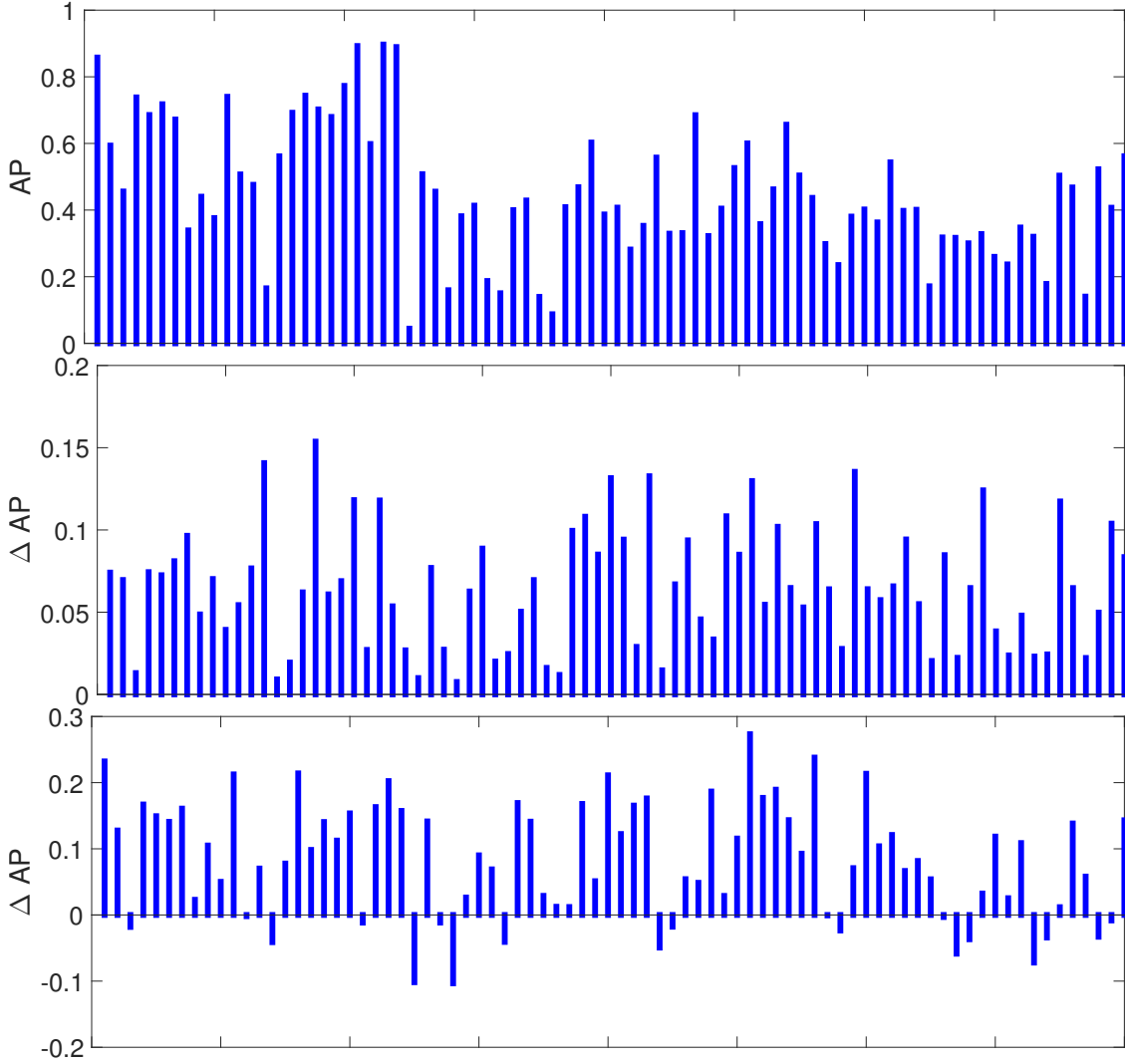


Figure 6. Per-class results on COCO. Top: category AP with our fusion method. Middle: Relative improvement by fusion with respect to masked boundary baseline  $S * B$ . Bottom: Relative improvement by fusion with respect to the segmentation baseline. Category names omitted to reduce clutter, the order matches standard COCO order.

- architecture for fast feature embedding. In *Proceedings of the ACM International Conference on Multimedia*, 2014. 4
- [14] L. Ladický, C. Russell, P. Kohli, and P. H. S. Torr. Associative hierarchical CRFs for object class image segmentation. In *ICCV*, 2009. 2
- [15] T.-Y. Lin, M. Maire, S. Belongie, J. Hays, P. Perona, D. Ramanan, P. Dollár, and C. L. Zitnick. Microsoft coco: Common objects in context. In *ECCV*. 2014. 2
- [16] J. Long, E. Shelhamer, and T. Darrell. Fully convolutional networks for semantic segmentation. In *CVPR*, 2015. 2
- [17] D. Martin, C. Fowlkes, D. Tal, and J. Malik. A database of human segmented natural images and its application to evaluating segmentation algorithms and measuring ecological statistics. In *ICCV*, 2001. 1
- [18] M. Mostajabi, P. Yadollahpour, and G. Shakhnarovich. Feed-forward semantic segmentation with zoom-out features. In *CVPR*, 2015. 2
- [19] J. Pont-Tuset, P. Arbeláez, J. Barron, F. Marques, and J. Malik. Multiscale combinatorial grouping for image segmentation and object proposal generation. In *arXiv:1503.00848*, March 2015. 2, 3
- [20] K. Simonyan and A. Zisserman. Very deep convolutional networks for large-scale image recognition. *arXiv preprint http://arxiv.org/abs/1409.1556*, 2014. 5
- [21] J. Uijlings and V. Ferrari. Situational object boundary detection. *arXiv preprint arXiv:1504.06434*, 2015. 1, 3, 4, 5, 6, 7
- [22] P. Yadollahpour, D. Batra, and G. Shakhnarovich. Discriminative re-ranking of diverse segmentations. In *CVPR*, 2013. 2
- [23] S. Zheng, S. Jayasumana, B. Romera-Paredes, V. Vineet, Z. Su, D. Du, C. Huang, and P. Torr. Conditional random fields as recurrent neural networks. *arXiv preprint arXiv:1502.03240*, 2015. 2